PCCP

ROYAL SOCIETY OF CHEMISTRY

PAPER

Published on 10 November 2026
Licensed under CC-BY 4.0

Check for updates

Cite this: DOI: 10.1039/d6cp03565e

Structure–property relations on exchange couplings in distorted halide-bridged Gd(III) complexes

Christian F. Pachl *[ab] and Karin Fink [a]

Received 8th September 2026,
Accepted 30th October 2026

DOI: 10.1039/d6cp03565e

rsc.li/pccp

In comparison to transition metals, the connection between the bridging geometry and the magnetic exchange coupling constant J remains vague for Gd(III)–Gd(III) magnetic couplings. However, such couplings are an important feature, for example for compounds showing a strong magnetocaloric effect. In this study, a series of Gd_2X_6 (X = F, Cl, Br, I) was systematically distorted and the magnetic coupling calculated using broken-symmetry DFT. We find an inversely exponential metal–metal distance dependence as well as the dependence on a second structural parameter, either the Gd–X distance or the Gd–X–Gd angle. We compared these structural dependencies with different DFT-features. We furthermore find that the nature of terminal ligands has neglectable influence. Using these results, we showed that such simple model complexes can be used to predict the coupling in experimentally investigated complexes with the same bridge. This lets us conclude that it may be possible to effectively extract reasonable exchange coupling constants and Spin-Hamiltonians for larger Gd(III)-clusters.

Introduction

Exchange interactions between Gd(III) ions are relevant for a number of applications as magnetic refrigerants,[1–6] as model systems for molecular magnets,[7–10] and as a possible platform for spin qubits.[11,12]

The half filled 4f-shell has a well defined $^8S_{7/2}$ ground state with only very small higher order spin–orbit contributions. Though the splitting of the ground state, which is typically below 1 cm^{-1},[13–15] is interesting for various applications such as qudits, MRT contrast agents and spin labeling in structural biology,[15–17] it plays a minor role for the determination of the exchange coupling. Thus, the ground state can be approximated to be isotropic.[18] This has several implications: Firstly, treating scalar relativistic effects is generally sufficient and spin–orbit coupling plays a minor role in comparison.[19–21] Secondly, dipolar interactions should not occur between the ground states of Gd(III) ions, therefore only isotropic exchange interactions are responsible for the cooperative phenomena in multinuclear Gd(III) molecules.[5]

However, even though a large number of compounds exhibiting 4f–4f exchange interactions have been reported in the past, well defined structure–property relations remain elusive. This is in contrast to exchange couplings in 3d-metal interactions where the Goodenough–Kanamori–Anderson rules indicate a clear relationship between the bridging angle and the coupling constants based on orbital symmetry and overlap.[22–24] This concept cannot be transferred to lanthanides given their predominantly ionic interaction with ligands.[25]

Due to the spin localization in the shielded 4f-orbitals, Gd(III) interactions follow a Heisenberg–Dirac–van Vleck Hamiltonian $\hat{H} = -2J_{ex}\hat{S}_1 \cdot \hat{S}_2$.[26–28] Here, a coupling constant J_{ex} couples two spins giving rise to a spin ladder for the total spin from $S_{tot} = S_1 + S_2 = 7$ to $S_1 - S_2 = 0$. However, this also means that the interaction strength is comparably small, usually well below 1 cm^{-1} compared to 3d-interactions which can be well above 100 cm^{-1}.[14,29]

The standard approach for investigating magnetic exchange interactions in the weak coupling regime is broken-symmetry density functional theory (BS-DFT) as originally proposed by Noodleman.[30] One first performs a single-point calculation on the high-spin (HS) state before localizing the unpaired orbitals and "flipping" the spin of those localized at one center subsequently performing a second single-point calculation. The original formula by Noodleman was generalized by Yamaguchi using a spin-projection approach in which a spin-contaminated determinant is projected onto pure M_S determinants.[31]

$$J_{ex} = \frac{E_{HS} - E_{BS}}{\langle S_{BS}^2 \rangle - \langle S_{HS}^2 \rangle} \quad (1)$$

The main advantage of using this formula is that it corrects for non-physical spin contamination of the density[31,32] in

[a] Institute of Nanotechnology (INT), Karlsruhe Institute of Technology (KIT), Kaiserstr. 12, 76131 Karlsruhe, Germany. E-mail: Christian.Pachl@kit.edu
[b] Institute of Inorganic Chemistry (AOC), Karlsruhe Institute of Technology (KIT), Kaiserstr. 12, 76131 Karlsruhe, Germany

comparison to other approaches.[30,33,34] Notably, it was recently shown that BS-DFT accumulates significant errors especially when covalent bonding is relevant for the exchange pathway.[32]

Structure property relations on Gd(III)-radical interactions have previously indicated a strong angle dependence.[35,36] Building upon studies by Rajeshkumar *et al.*[21] and Roy *et al.*,[37] we have recently performed a large comparative benchmark on 27 dinuclear Gd(III) compounds probing the influence of various DFT options on the results of BS-DFT calculations in comparison to fitted experimental data.[14] We concluded that the parallel use of four functionals, namely pbe0, bh-lyp, cam-b3lyp and ωb97-x, will generally result in errors smaller than 0.02 cm^{-1} when used with sufficiently large basis sets. We also compared structural parameters in the testbed with the computed (and fitted) parameters and found that no overarching relationship could be reported relating the Gd–Gd distance and Gd–L–Gd bridging angle with the coupling constant. It was only possible to show a weak correlation between the Gd–Gd distance and J_{ex} for similarly bridged molecules.

Halide bridged Gd(III) complexes are readily discussed in literature. The simplicity of the bridge makes them an ideal testbed for structure property relationship studies. A number of possible bridging motifs have been reported in the past (Fig. 1): at two instances linear fluoride bridges between two trivalent Gd(III) ions have been reported.[38,39] The most common bridging motif, *via* two halides, has been published for fluorides,[40–42] chlorides,[43–47] bromides[48,49] and iodides.[50,51] There is only one instance where the metals were bridged *via* three chlorides.[52] Also, larger compounds have been established such as tri-[53] and tetranuclear clusters.[54,55]

In this study we explore this relationship in simple model systems that allow for a detailed analysis of which structural parameters are relevant for the intramolecular coupling between Gd(III) ions. To do this, we computed the coupling in distorted Gd_2X_6 (X = F, Cl, Br, I) D_{2h} symmetric, neutral molecules (Fig. 2). The structure of these molecules has been previously studied in the gas phase.[56] Theoretical studies, *e.g.* by Kovács in 2000, focused on their bonding and electronic structure and vibrational properties but not on the magnetic coupling.[57,58] Though no magnetic experimental reference data are available, their simplicity makes them ideal for the current study.

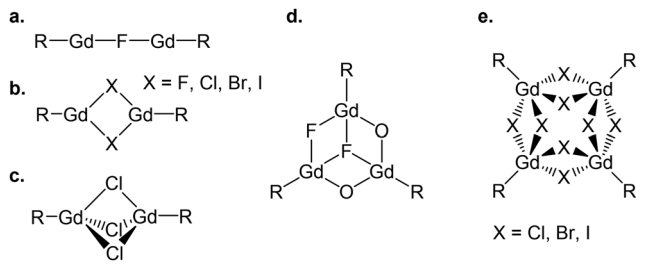


Fig. 1 Different reported bridging motifs for Gd(III) dimers: (a) linear Gd–F–Gd bridges, (b) two μ_2 bridging halide ions, (c) bridges *via* three chlorides, (d) O- and F-bridged triangles, (e) Gd_4X_8 squares.

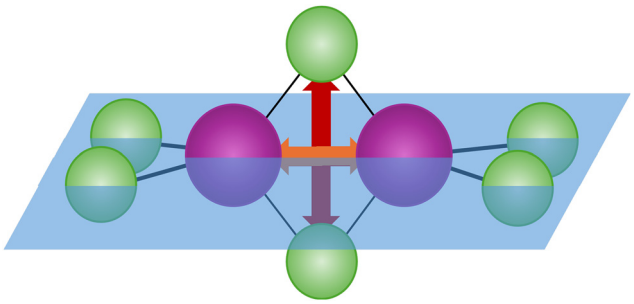


Fig. 2 Schematic of the Gd_2X_6 (X = F, Cl, Br, I) molecule in D_{2h}-symmetry. The orange arrow indicates the distortion of the two in-plane GdX_2 moieties while the red arrow indicates the distortion of the two μ_2 bridging X ions.

Methods

In a first step, the molecular structure of Gd_2Cl_6 was optimized on a bh-lyp-DKH2/rij/x2c-TZVPall level of theory using Turbomole 7.8 resulting in a D_{2h} symmetric structure for the $S = 7$ state.[59–63] Vibrational frequencies were computed to validate the convergence to a minimum.

To probe different structure–property relations between the bridging geometry and exchange coupling constant, we distorted this structure along two parameters. The Gd–Gd distance was altered by moving the two in-plane GdX_2-moities closer/apart.

The bridging X–X distance was altered by moving the respective ions closer/further to the Gd–Gd connection axis. This elongation and compression was performed in seven steps of 5.29 pm (0.1 a_0) in each direction leading to a 15 × 15 grid of distorted structures. At each of these points, a HS and a BS-DFT calculation were performed to extract J (eqn (1)) using the functionals pbe0,[64] bh-lyp,[62] cam-b3lyp[65] and ωb97-x[66] and otherwise the same parameters as in the geometry optimization. For the computation of Gd_2F_6, Gd_2Br_6, and Gd_2I_6 dimers the same coordinates as for Gd_2Cl_6 were used without further optimization. Doing so, all four molecules can be compared on the same grid even if the optimized structure is not necessarily on it.

This distortion scheme allows to probe four structural parameters against the coupling constant: the Gd–Gd distance, the X–X distance, the Gd–X distance and Gd–X–Gd bridging angle. Since the terminal halides remain fixed, X will for now always refer to the bridging ions unless explicitly noted otherwise.

Symbolic regression on the four geometrical parameters was performed using Python 3.15.5 and the PySR package.[67] Symbolic regression algorithms are genetic machine learning algorithms aimed to reproduce a set of observables by connecting a set of features with human interpretable equations. Here, each such equation has a given complexity, which is the sum of variables and mathematical operators. *E.g.*, a formula such as "$A + 5$" would have a complexity of 3, "$((A \times B) + C)/\exp(D)$" a complexity of 8. The algorithm randomly initializes a number of such equations before evaluating their suitability. Afterwards, the best equations are taken and mutated by either

 This journal is © the Owner Societies 2026

introducing new variables or mixing expressions from different expression trees, forming the next generation. For a more detailed description of the algorithm we refer to ref. 67. Notably, genetic algorithms can be used to predict new molecules or to find global minima in structure optimization problems.[68,69]

Upon normalization using the pandas StandardScaler,[70] geometrical dependencies were investigated using 30 populations of size 40 and converged for 3000 iterations limiting the maximum complexity to 15. The starting equations are randomly generated. Furthermore, the unary operators "exp", "log", "cos", "sin", and "tan" were used limiting the maximum complexity within the trigonometric operators to three. Equations are chosen according to PySR's implicit "best" model selection.

Subsequently, additional structures were investigated where the terminal and bridging ligands were replaced and reoptimized when explicitly mentioned:

First, we investigated mixed halide structures of the formula $Gd_2X_4Y_2$, where X denotes terminal and Y denotes bridging halides. All of these structures were optimized with the functionals pbe0, bh-lyp, cam-b3lyp and ωb97-x respectively with an x2c-TZVPall basis, rij approximation and scalar relativistic X2C. We note, that while the geometry optimization was carried out using 1c-X2C, the BS-DFT calculation was computed with DKH2. This, however is not expected to make a notable difference.

To keep the same bridging atom, but change its electronic structure, we started with the Gd_2Cl_6 structure and replaced the bridging ions by hypohalites and hydroxy functions to arrive at models $Gd_2Cl_4(OX)_2$ (X = F, Cl, Br, I, H). Again, these were optimized with the previously indicated methods. In this case, we then performed an additional analysis by keeping the relaxed $Gd_2Cl_4O_2$ atoms fixed and replacing the halide of the hypohalites to the other four. *E.g.* the relaxed structure of $Gd_2Cl_4(OF)_2$ was taken, F replaced to Cl, Br, I, H and only the latter atoms were reoptimized. The aim of this study was to separate the electronic influences of the halides from the geometry influences on the bridge.

Results and discussion I: exchange coupling in distorted structures

The optimization of the Gd_2Cl_6 molecule yielded a D_{2h}-symmetric molecular structure. The obtained Gd–Gd distance is 404.9 pm. The Gd–Cl distances are 247.4 pm and 269.8 pm which are similar to the shorter Gd–Cl distances in the $GdCl_3$ crystal structure.[71] The structure is schematically shown in Fig. 2.

The heatmap of J_{ex} resulting from the distorted calculation is shown exemplary for the Gd_2Cl_6 molecules in Fig. 3. At short Cl–Cl distances, the coupling is always antiferromagnetic while at large Cl–Cl distances, the coupling is always ferromagnetic. The coupling increases in magnitude towards lower Gd–Gd distances while approaching 0 cm^{-1} at large distances. The J = 0 cm^{-1} line

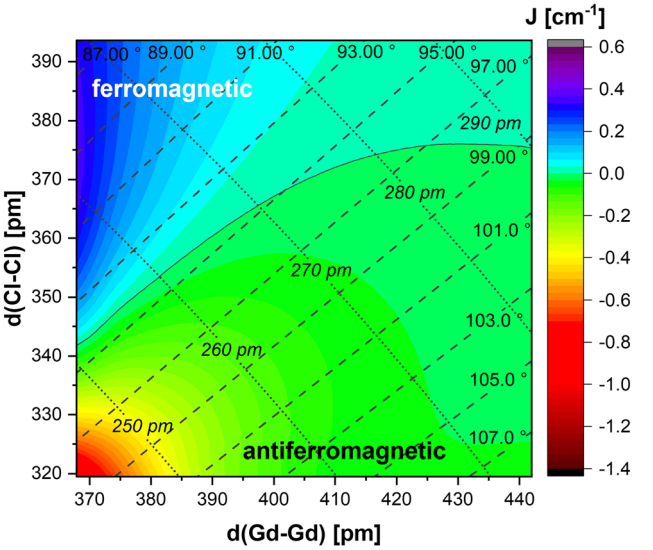


Fig. 3 Heat map for the exchange coupling constant calculated with bh-lyp for the 15 × 15 grid for the Gd_2Cl_6 molecule. The *x*-axis is the Gd–Gd distance, *y*-axis is the Cl–Cl distance. The Gd–Cl–Gd angle is indicated by dashed lines, the Gd–Cl distance by dotted lines. The solid line indicates J = 0 cm^{-1}. Blue colors indicate ferromagnetic, red colors antiferromagnetic coupling constants.

first follows approximately the Gd–Cl–Gd = 94° angle before deviating significantly at larger Gd–Gd distances. Qin *et al.* found such an intersection for $Gd_2(OH)_2$-moieties at around 118.9°.[72]

The sign change of the exchange coupling constants with varying bridging angle has been investigated previously for 3d-compounds where it was connected to a reduction of the antiferromagnetic contribution to the coupling when the orbitals get orthogonal.[73,74] In fact, it is a key feature of the Good-enough–Kanamori–Anderson rules.[24]

Furthermore, the heat maps for Gd_2F_6, Gd_2Br_6 and Gd_2I_6 as well as those for the functionals pbe0, cam-b3lyp and ωb97-x are structurally similar to that for Gd_2Cl_6 (bh-lyp) and are shown in Fig. S1–S5. The coupling constants become stronger from F < Cl < Br < I. This is not surprising considering that the Gd–X distances in this grid feature very long Gd–F contacts and very short Gd–I distances.

No straightforward deductions can be made by comparing J with the individual parameters in this testbed. This is exemplified in Fig. S6 for the data for Gd_2Cl_6 with bh-lyp. All four parameters show a distinct and non-linear behavior with respect to J. To disentangle these relationships, we modeled the resulting coupling constants using symbolic regression.[67] This genetic algorithm provides human interpretable expressions to reconstruct an observable (J) from a set of features. The resulting expressions for the four investigated molecules are summarized in Table S1.

The most notable observation is that for most given complexities the best equation found is dependent on an exponential decay of either the Gd–Gd distance and/or the Gd–X distance. We want to exemplify this by fitting a simple exponential of the form $J = J_0 + Ae^{-B \cdot d(\mathrm{Gd-Gd})}$ to three horizontal lines in Fig. 3 as shown in Fig. 4. Fit parameters are provided in

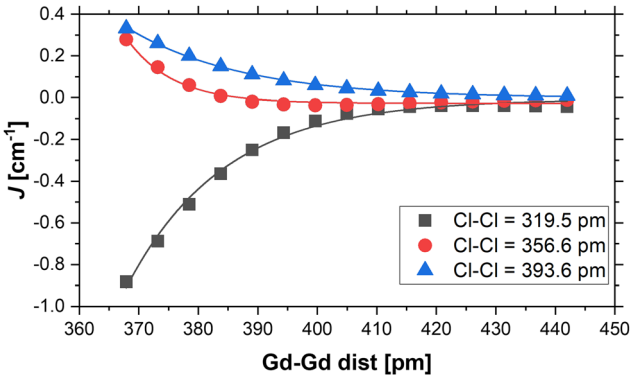


Fig. 4 Three exemplary fits with constant Cl–Cl distance and variable Gd–Gd distance using a simple three-parameter exponential. The reference data are from BS-DFT calculation on Gd_2Cl_6 with the functional bh-lyp.

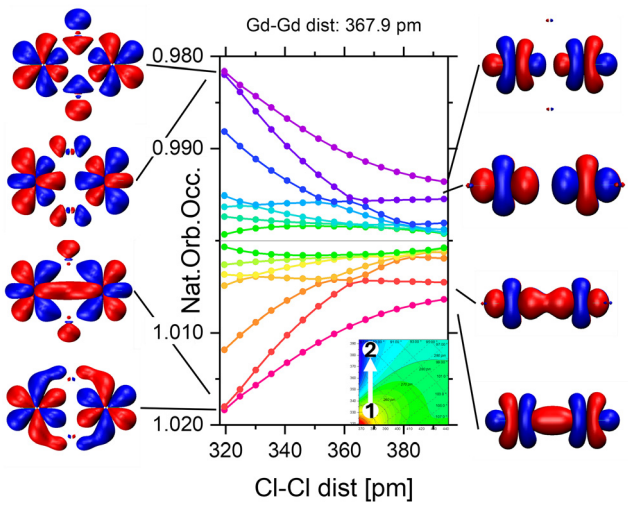


Fig. 5 In the BS-state, there are 14 natural orbitals with occupation numbers close to 1. Their occupation number (*y*-axis, Nat. Orb. Occ.) is shown here against the Cl–Cl distance (*x*-axis) in Gd_2Cl_6 at the shortest Gd–Gd distance. The lowest and highest two orbitals are plotted with an isodensity of 0.01. The inset shows which line in the 15 × 15 grid is shown here.

Table S2. The excellent agreement indicates the importance of the Gd–Gd distance. Yet, this simple model cannot explain intersections with zero. Furthermore, we want to stress that this formula is empirically based on the general structure obtained from symbolic regression and do not want to physically interpret each of the parameters.

Similar results were previously reported by different groups for M–O–M bridges, where M = Ti(III), Cr(III), Fe(III).[75–77] However, in each case, linear M–O–M arrangements were investigated. Interestingly, Koroteev *et al.* found a maximum of *J* around 425 pm when analyzing the data of 34 Gd_2O_2-bridged compounds and thus fitted the *J*-distance dependence with a fourth order power law.[78] While the angle dependence was not investigated in this study, these results are not at odds with the findings reported here. In fact, the calculations on Gd_2F_6 (Fig. S1) indicate that such a dependency can be constructed considering that real chemical compounds are not distributed uniformly on this grid but are constrained to reasonable bond distances and angles.

Next, we want to investigate common DFT indicators on this grid. Corresponding spin orbitals (CSOs) are a set of orbitals obtained by rotating the α- and β-orbitals maximizing their overlap. When this analysis is performed on a BS-state where α- and β-spin densities are localized to different centers, one obtains 2 × 7 CSOs with overlaps S(a,b) significantly differing from 1. These are the magnetic orbitals carrying the unpaired spin density and thus the ones that are relevant for magnetic exchange. CSOs have been used in the past to rationalize antiferromagnetic exchange.[7,21,79] When the magnetic orbitals are predominantly 4f-orbitals, this value is expected to be extremely dependent on the Gd–Gd distance. However, a very small overlap would be expected considering that the inter-lanthanide distance is always significantly larger than the sum of van der Waals radii.[80] In the following, we will use the trace of the overlap matrix between the CSOs localized at either center from the BS state as a measure of total overlap.

Notably, the CSO overlap is only significant at low Gd–Gd and Cl–Cl distances (Fig. S7) and thus inversely correlated with the Gd–Cl distance (spearman correlation $r_S = -0.966$, Fig. S8). To interpret this result, it is convenient to switch to a closely related metric which is the occupation number of the natural orbitals in the BS-state (Fig. S9). In the BS-state, there are 14 orbitals with occupation numbers close to 1. These can be related to bonding and antibonding combinations between the localized magnetic orbitals. The "more bonding" such a pair is, the more the natural orbital occupation numbers deviate from 1. This is shown in Fig. 5 for the 15 models with the shortest Gd–Gd distance (367.9 pm) and varying Cl–Cl distances (*x*-axis, also schematically shown as the inset of Fig. 5). It becomes apparent that the interaction with the ligands leads to significantly stronger orbital interactions between magnetic orbitals. Similar conclusions were drawn from multireference calculations in the past.[81,82]

This shows that a short bond between the interacting metals and the bridge can facilitate stronger antiferromagnetic interactions through stronger orbital overlap.

The occupation of the Gd 5d orbitals according to Natural Population Analysis (NPA)[83] was used in the past to argue for charge transfer contributions to the coupling constant in several studies.[84,85] While we did not find a general correlation with *J* in our previous study,[14] we want to add here that this metric is non-linearly correlated with the cso-trace ($r_S = 0.999$, Fig. S10).

Results and discussion II: influence of the bridge *vs.* terminal ligands

Changing bridging ligand and terminal ligands independently may give indications about the relevance of either to the coupling. Starting from the Gd_2Cl_6 structure, terminal and

 This journal is © the Owner Societies 2026

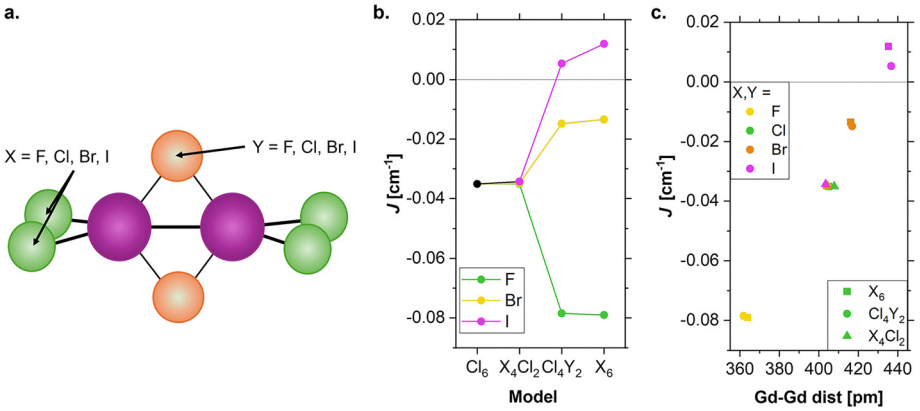


Fig. 6 (a) Schematic view of the $Gd_2X_4Y_2$ testbed. (b) J against the different models where the terminal and/or the bridging ions were replaced and the structure subsequently reoptimized. (c) J of the nine $Gd_2X_4Y_2$ against the Gd–Gd distance.

bridging ions were replaced by other halides (Fig. 6a) and the structure subsequently reoptimized. For the resulting $Gd_2X_4Y_2$ a BS-DFT calculation was performed to obtain J.

The replacement of terminal ligands did not yield a notable change in the coupling constant (Fig. 6b). In contrast, when the bridging halide was replaced and optimized, a significant change could be observed. Going from Cl^- to F^-, J became significantly more antiferromagnetic, while it became smaller when replaced to Br^-. In the case of I^-, the coupling turned weakly ferromagnetic. Notably, this was not the case for the pbe0 functional where J for iodide bridged structures remained weakly antiferromagnetic (Fig. S11). One has to consider that by reoptimizing the structure, the entire bridging geometry changed. Plotting the coupling constants against the Gd–Gd distance (Fig. 6c), one clearly observes the trend already established, where a larger Gd–Gd distance results in a more ferromagnetic coupling.

Comparing halide bridges, this means that the coupling constant becomes more ferromagnetic from F^- to I^-, in the equilibrium geometries. However, if the geometry is fixed the absolute coupling constant increases from F^- to I^-.

The most common bridging atom by far for Gd-dimers is negatively charged oxygen atoms.

To mimic the changes of different substituents on this atom, we subsequently investigated a set of hypohalite bridged Gd dimers by replacing the bridging ions with OX^- ions (X = H, F, Cl, Br, I) while retaining D_{2h} symmetry. This being said, we are not aware of any instances where it was possible to crystallize hypohalite-Gd(III) salts in experiment.

The results of these calculations can be found in Fig. 7. While previously reported trends can be found here as well (*e.g.* bh-lyp resulting in the most positive coupling constant), a significant dependency of J on the hypohalite bridge can be observed. Notably, the calculation with ωb97-x resulted in a value significantly deviating from the trend, but also the frequency calculation failed for this geometry and we thus only included the value for completeness.

The majority of this trend can be again explained through changes in the bridging geometry where the Gd–Gd distance changes from 393.7 pm (OF^-) to 364.5 pm (OI^-). OH^- is an outlier here, as it has a Gd–Gd distance of 361.6 pm but a coupling constant between that of OCl^- and OBr^-. The same trend is observed in comparison to the Gd-O distances.

To eliminate the influence of the bridge's geometric relaxation, we subsequently fixed all atomic coordinates but the halide in the hypohalite and replaced it for all structures with the other 4 halides and/or hydrogen only optimizing the O–X distance. *E.g.* the base structure of $Gd_2Cl_4(OF)_2$ was taken, F replaced to Br and only the Br position reoptimized to get reasonable O-Br distances.

The results are shown in Fig. 8 and Fig. S12. It becomes clear that the geometric distortion of the bridge is more influential than the residue on the bridging oxygen. This is especially interesting considering that the induced electronic changes are quite extreme compared to common bridges where for example only a residue on a phenolate would alter. Furthermore, it can be noted that these differences can be related to the overlap of CSOs. A larger overlap of CSOs generally leads to more antiferromagnetic coupling.

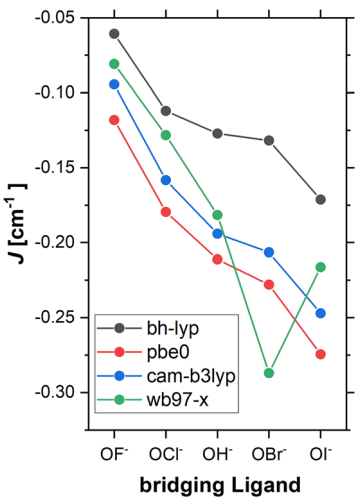


Fig. 7 Computed exchange coupling constants for $Gd_2Cl_4(OX)_2$ (X = H, F, Cl, Br, I) structures. Geometries were optimized with the same functional used for the BS-DFT calculation.

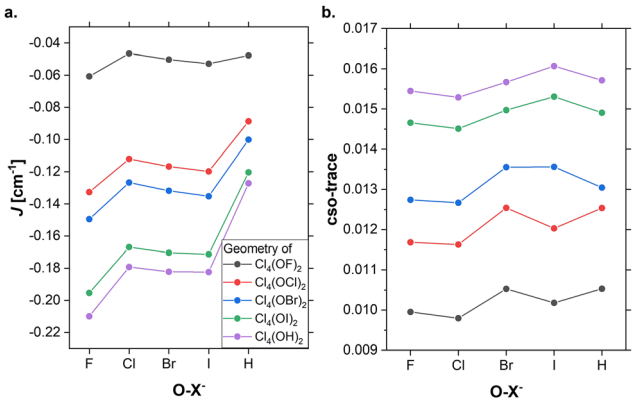


Fig. 8 Exchange coupling constants and CSO-overlaps for the 25 generated $Gd_2Cl_4(OX)_2$ (X = H, F, Cl, Br, I). Here, only the halogen of the hypohalite was replaced and reoptimized for all 5 previously optimized structures. These results are for the bh-lyp functional. (a) Coupling constant against hypohalite, (b) CSO orbital overlap against hyphalite.

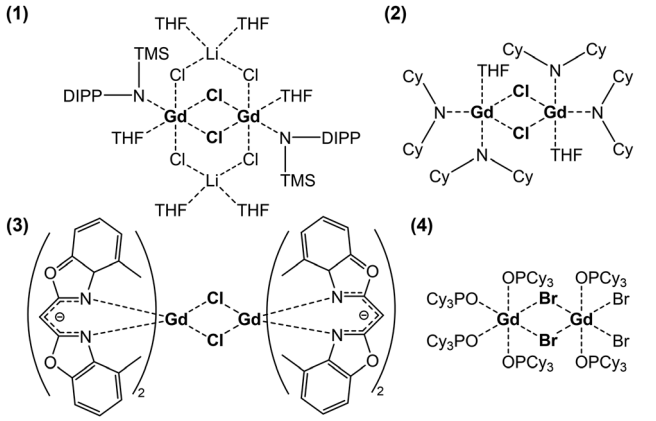


Fig. 9 Scheme of molecular structures for compounds (**1**)–(**4**). THF = tetrahydrofuran, DIPP = diisopropylphenyl, TMS = trimethylsilyl, Cy = cyclohexyl, $OPCy_3$ = tricyclohexylphosphone oxide.

Summarizing this section, we want to emphasize that the bridging geometry is more influential on the coupling constant than the residue on the bridging atom and significantly more than the changes on terminal ligands. Based on these results we hypothesize, in agreement with a conclusion drawn by Roy *et al.*,[37] that changes of substituents of bridging alcoholates and carboxylates are also negligible. A recent study by Fellner *et al.* showed a relation between bridging carboxylic acid's Hammett constant and the coupling constant.[86] In conjunction with the findings here, this indicates that while not directly influencing the exchange coupling, the electronic structure of the ligand may influence the geometry and therefore indirectly *J*.

Results and discussion III: application to halide bridged Gd-complexes

We subsequently tested how transferable these results are in comparison to magnetically investigated dihalide bridged molecules. Unfortunately, only very few such molecules are magnetically characterized. Compounds (**1**),[43] (**2**)[45] and (**3**)[47] are bridged *via* two chlorides, compound (**4**)[49] is bridged *via* two bromide ions (Fig. 9 and Fig. S13–S16).

We have previously computed the exchange coupling for (**1**) and (**2**).[14] Thus, only calculations on compounds (**3**) and (**4**) had to be performed. The computed coupling constants as well as the relevant structural parameters are summarized in Table 1.

In general, the agreement between BS-DFT and fitted values is acceptable and in the range of previously discussed errors.[14] BS-DFT underestimates the coupling in (**1**) significantly by a factor of $\frac{1}{2}$. The coupling is also underestimated for compound (**2**) with errors well within DFT accuracy. For compound (**3**) the computations give a range around the fitted value and are in excellent agreement. Lastly, for compound (**4**), the coupling is slightly overestimated, although the bh-lyp functional is in excellent agreement with the experiment.

While these results reiterate that BS-DFT provides reasonable results, we wanted to explore whether it is possible to approximate the coupling constant from the bridging geometry directly. To do so, we took the 2D plots (Fig. 3 and Fig. S1–S4) and simply extracted the value at the grid point closest to the molecular geometry (Table 1).

Surprisingly, these results are always closer to the experimental values for compounds (**2**), (**3**) and (**4**) with the functionals bh-lyp, pbe0 and cam-b3lyp. This is not the case for (**1**) and the ωb97-x functional. The latter is not surprising considering that this functional has more or less consistently deviated qualitatively from the others in this study. We note here that the Gd_2Cl_2 rhombus in (**1**) is significantly distorted from the ideal equilateral shape with the Gd–X distances differing by 24 pm, significantly more than for the other molecules. Thus, a projection onto an idealized shape is not expected to work as well.

These results are intriguing as they indicate that it is possible to approximate the exchange coupling between halide bridged Gd(III) ions straightforwardly from extremely simplified model systems.

Conclusion

Thus, we conclude this comprehensive study on simple Gd_2X_6 model structures for intramolecular exchange coupling.

1. We find that the underlying structure–property relationships are not dominated by a single structural parameter. Rather, symbolic regression of coupling constants obtained from distorted model structures suggests that *J* is inversely exponentially dependent on the Gd–Gd and Gd–X distances. At short Gd–Gd distances and short Gd–X distances, the coupling is strongly antiferromagnetic and turns ferromagnetic at short Gd–Gd but long Gd–X distances. Because the Gd–X distances are generally in a narrow range, this effectively renders the coupling a balance between the Gd–Gd distance and the Gd–X–Gd angle. Keeping the Gd–X distance fixed, the Gd–X–Gd angle will be acute for short Gd–Gd distances and therefore strongly

This journal is © the Owner Societies 2026

Table 1 Relevant structural parameters and reference and computed exchange coupling constants for compounds (**1**)–(**4**). The angle refers to the Gd–X–Gd angle. All coupling constants are given in cm^{-1}. Experimental reference values were taken from the respective publications. J_{ref} refers to values approximated from the 2D plots. * BS-DFT calculations for compounds (**1**) and (**2**) are taken from ref. 14

	(**1**)	(**2**)	(**3**)	(**4**)
Gd–Gd dist [pm]	4.376	4.303	4.302	4.513
Angle [°]	102.6	102.6	104.5/103.3	99.5/100.8
Gd–X dist [pm]	268.1/292.3	274.3/277.1	272.8-274.8	286.3-304.9
J_{exp}	−0.09 (ref. 43)	−0.037 (ref. 45)	−0.035 (ref. 47)	−0.015 (ref. 49)
$J_{bh\text{-}ly}$	−0.029*	−0.013*	−0.025	−0.020
J_{pbe0}	−0.054*	−0.027*	−0.050	−0.043
$J_{cam\text{-}b3lyp}$	−0.051*	−0.025*	−0.044	−0.041
$J_{\omega b97\text{-}x}$	−0.045*	−0.020*	−0.035	−0.036
$J_{bh\text{-}lyp,ref}$	−0.022	−0.022	−0.026	−0.015
$J_{pbe0,ref}$	−0.041	−0.041	−0.044	−0.034
$J_{cam\text{-}b3lyp,ref}$	−0.028	−0.028	−0.030	−0.022
$J_{\omega b97\text{-}x,ref}$	−0.006	−0.006	−0.004	−0.003

ferromagnetic, whereas a large Gd–Gd distance correlates with an obtuse angle and therefore weak antiferromagnetic coupling. Notably deviating from this trend would require unusual Gd–X distances.

2. For compressed Gd–X and Gd–Gd distances, a strong increase in the overlap of corresponding spin orbitals is accompanied by a strongly antiferromagnetic interaction. This furthermore coincides with a more predominant mixture of 4f- and ligand orbitals. A correlation can be noted with respect to NPA occupations of Gd 5d orbitals suggesting that these parameters are (at least in DFT calculations) not independent.

3. By replacing the terminal and bridging ligands independently, we found that the terminal ligands only have an insignificant influence on the coupling constant while structural changes in the bridge alter the coupling constant much more.

4. We employed hypohalite (OX^-, X = H, F, Cl, Br, I) bridging ligands as model systems to keep one bridging atom and only changing the electronic parameters indirectly through the halide. As observed before, this led us to hypothesize that the residues on bridging alcoholates only marginally influence the coupling constant electronically and are more important to tailor the bridging geometry.

5. Finally, we compared a set of halide bridged Gd(III) complexes to the coupling constants obtained for the model cluster with a similar bridging geometry. We found good agreement between the calculations for the model clusters and full complexes. Moreover, excellent agreement with experiment could be obtained.

The implications of this study are relevant to different areas of molecular magnetism. First, this approach could aid in constructing Gd(III) clusters with very strong MCE. Coupling constants for large, multinuclear Gd(III) clusters, for which BS-DFT is not accessible, can be inexpensively approximated by extending the present study to oxygen bridges and computing a larger set of distorted model structures of Gd(III) dimers. Secondly, we are not aware of any ferromagnetically coupled, chloride bridged Gd(III) coupling experimentally observed. To achieve ferromagnetic coupling, one would need to compress the Gd–Gd distance notably while keeping the same Gd–Cl distance. Thirdly, this study may help to understand when exchange coupling competes with dipolar coupling in other 4f-based molecular magnets. Considering that the direction of magnetic anisotropy and therefore the dipolar coupling is well understood, this study may guide the rational design of both types of coupling in combination.

Author contributions

C. F. P. conceptualization, data curation, formal analysis, investigation, visualization, writing – original draft; K. F. formal analysis, funding acquisition, supervision, writing – review & editing.

Conflicts of interest

There are no conflicts to declare.

Data availability

The data that supports the findings of this study are available within the article and the supplementary information (SI). Supplementary information: additional graphs for data referenced but not shown in the main manuscript such as calculations with different functionals or other halide combinations. Furthermore, fitting parameters, correlation diagrams and pictures of the computed molecules are provided. See DOI: https://doi.org/10.1039/d6cp03565e.

Coordinates for all molecules optimized within this study are available on KIT Open free of charge. See DOI: https://doi.org/10.35097/89qyjssv5324ym7c.

Acknowledgements

We would like to thank Dr Dominik Steinmetz for a program to compute the CSO overlap matrix. We also thank the CRC1573 ''4f for future'' and the Landesgraduiertenförderung of the state Baden-Württemberg for funding this project.

References

1 T. G. Tziotzi, D. Gracia, S. J. Dalgarno, J. Schnack, M. Evangelisti, E. K. Brechin and C. J. Milios, A $\{Gd_{12}\ Na_6\}$ Molecular Quadruple-Wheel with a Record Magnetocaloric Effect at Low Magnetic Fields and Temperatures, *J. Am. Chem. Soc.*, 2023, **145**, 7743–7747.

2 J. Braun, D. Seufert, C. E. Anson, J. Tang and A. K. Powell, An Effectively Uncoupled Gd8 Cluster Formed through Fixation of Atmospheric CO_2 Showing Excellent Magnetocaloric Properties, *Int. J. Mol. Sci.*, 2023, **25**, 264.

3 J. W. Sharples, Y.-Z. Zheng, F. Tuna, E. J. L. McInnes and D. Collison, Lanthanide discs chill well and relax slowly, *Chem. Commun.*, 2011, **47**, 7650.

4 A. M. Tishin and Y. I. Spichkin, *The Magnetocaloric Effect and its Applications*, CRC Press, Boca Raton, 1st edn, 2003.

5 Y.-Z. Zheng, G.-J. Zhou, Z. Zheng and R. E. P. Winpenny, Molecule-based magnetic coolers, *Chem. Soc. Rev.*, 2014, **43**, 1462–1475.

6 J. W. Sharples, D. Collison, E. J. L. McInnes, J. Schnack, E. Palacios and M. Evangelisti, Quantum signatures of a molecular nanomagnet in direct magnetocaloric measurements, *Nat. Commun.*, 2014, **5**, 5321.

7 M. Liu, Y.-C. Chen, A. Mondal, H. Wang, M.-L. Tong, R. A. Layfield and F.-S. Guo, η^6-Benzene Tetra-Anion Complexes of Early and Late Rare-Earth Metals, *J. Am. Chem. Soc.*, 2025, **147**, 11359–11367.

8 M. Machata, R. Herchel, I. Nemec and Z. Trávníček, Crystal structures and magnetic properties of two series of phenoxo- *O* bridged dinuclear Ln_2 (Ln = Gd, Tb, Dy) complexes, *Dalton Trans.*, 2017, **46**, 16294–16305.

9 J. Xiong, H.-Y. Ding, Y.-S. Meng, C. Gao, X.-J. Zhang, Z.-S. Meng, Y.-Q. Zhang, W. Shi, B.-W. Wang and S. Gao, Hydroxide-bridged five-coordinate DyIII single-molecule magnet exhibiting the record thermal relaxation barrier of magnetization among lanthanide-only dimers, *Chem. Sci.*, 2017, **8**, 1288–1294.

10 H. Wang, C. Liu, T. Liu, S. Zeng, W. Cao, Q. Ma, C. Duan, J. Dou and J. Jiang, Mixed (phthalocyaninato)(Schiff-base) di-dysprosium sandwich complexes. Effect of magnetic coupling on the SMM behavior, *Dalton Trans.*, 2013, **42**, 15355–15360.

11 F. Luis, P. J. Alonso, O. Roubeau, V. Velasco, D. Zueco, D. Aguilà, J. I. Martínez, L. A. Barrios and G. Aromí, A dissymmetric $[Gd_2]$ coordination molecular dimer hosting six addressable spin qubits, *Commun. Chem.*, 2020, **3**, 176.

12 E. Palacios, D. Aguilà, D. Gracia, D. Maniaki, L. A. Barrios, A. Chiesa, J. I. Martínez, V. Novikov, O. Roubeau, S. Carretta, M. Evangelisti, G. Aromí and F. Luis, Self-Cooling Molecular Spin Qudits, *Adv. Mater.*, 2025, e11061.

13 S. Khan, V. Peters, J. Kowalewski and M. Odelius, Zero-field splitting in the isoelectronic aqueous Gd(III) and Eu(II) complexes from a first principles analysis, *Chem. Phys.*, 2018, **503**, 56–64.

14 C. F. Pachl, J. Braun, C. E. Anson and K. Fink, A Gd-Dimer Benchmark Study: Is DFT an accurate Method for the Prediction of Gadolinium Exchange Coupling Constants, *Magnetochemistry*, 2026, **12**, 67.

15 C. Rodríguez-Esteban, E. Ruiz-Bilbao, J. Bustamante-Fernández, F. Tuna, L. Lezama, A. Mailman, A. Ullah, A. Gaita-Ariño, B. Artetxe, M. Gonidec and I. Oyarzabal, Coherent Spin Manipulation in Mononuclear Gadolinium-Substituted Polyoxometalate–Organic Hybrids, *J. Phys. Chem. Lett.*, 2025, **16**, 3072–3077.

16 M. Benmelouka, A. Borel, L. Moriggi, L. Helm and A. E. Merbach, Design of Gd(III)-Based Magnetic Resonance Imaging Contrast Agents: Static and Transient Zero-Field Splitting Contributions to the Electronic Relaxation and Their Impact on Relaxivity, *J. Phys. Chem. B*, 2007, **111**, 832–840.

17 A. Bogdanov, V. Frydman, X.-C. Su, M. Seal, W. Zhu, A. M. Gronenborn, A. Schnegg and D. Goldfarb, Unlocking Gd(III) Anisotropy:Determining the Zero-FieldSplitting Axes to Enhance Spin-Label Structural Analysis, *J. Am. Chem. Soc.*, 2026, **148**, 23597–23610.

18 D. Schray, D. Westerbeck, J. Braun, Y. Lan, S. Gómez-Coca, W. Wernsdorfer, E. Ruiz, C. E. Anson, J. Schnack and A. K. Powell, Fe–Gd Ferromagnetic Cyclic Coordination Cluster $[Fe^{III}{}_4Gd^{III}{}_4\ (teaH)_8(N_3)_8(H_2O)]$ with Magnetic Anisotropy–Theory and Experiment, *Inorg. Chem.*, 2023, **62**, 6642–6648.

19 R. Essajai, N. Ennassiri, M. Balli, M. Zidane, E. Salmani, O. Mounkachi, M. Rouchdi, A. Abbassi, H. Ez-Zahraouy, A. Mzerd and N. Hassanain, Revisiting the magnetic and magnetocaloric properties of bulk gadolinium: A combined DFT and Monte Carlo simulations, *Phys. Scr.*, 2020, **96**, 015808.

20 G. Rajaraman, F. Totti, A. Bencini, A. Caneschi, R. Sessoli and D. Gatteschi, Density functional studies on the exchange interaction of a dinuclear Gd(III)-Cu(II) complex: method assessment, magnetic coupling mechanism and magneto-structural correlations, *Dalton Trans.*, 2009, 3153–3161.

21 T. Rajeshkumar, S. K. Singh and G. Rajaraman, A computational perspective on magnetic coupling, magneto-structural correlations and magneto-caloric effect of a ferromagnetically coupled {GdIII–GdIII} Pair, *Polyhedron*, 2013, **52**, 1299–1305.

22 P. W. Anderson, Antiferromagnetism. Theory of Superexchange Interaction, *Phys. Rev.*, 1950, **79**, 350–356.

23 J. B. Goodenough, Theory of the Role of Covalence in the Perovskite-Type Manganites [La, M(II)]MnO_3, *Phys. Rev.*, 1955, **100**, 564–573.

24 J. Kanamori, Superexchange interaction and symmetry properties of electron orbitals, *J. Phys. Chem. Solids*, 1959, **10**, 87–98.

25 S. P. Sinha, in *Rare Earths*, Springer Berlin Heidelberg, Berlin, Heidelberg, 1977, vol. 25, pp. 69–149.

26 P. A. M. Dirac, *The Principles of Quantum Mechanics*, Clarendon Press, Oxford, 3rd edn, 1947.

27 W. Heisenberg, Zur Theorie des Ferromagnetismus, *Z. Phys.*, 1928, **49**, 619–636.

28 J. H. Van Vleck, *The Theory of Electric and Magnetic Susceptibilities*, Oxford University Press, 1932.

29 J. J. Phillips and J. E. Peralta, Magnetic Exchange Couplings from Semilocal Functionals Evaluated Nonself-Consistently

 This journal is © the Owner Societies 2026

on Hybrid Densities: Insights on Relative Importance of Exchange, Correlation, and Delocalization, *J. Chem. Theory Comput.*, 2012, **8**, 3147–3158.
30 L. Noodleman, Valence bond description of antiferromagnetic coupling in transition metal dimers, *J. Chem. Phys.*, 1981, **74**, 5737–5743.
31 T. Onishi, D. Yamaki, K. Yamaguchi and Y. Takano, Theoretical calculations of effective exchange integrals by spin projected and unprojected broken-symmetry methods. I. Cluster models of K2NiF4-type solids, *J. Chem. Phys.*, 2003, **118**, 9747–9761.
32 N. Iwahara, Z. Huang, A. Mansikkamäki and L. F. Chibotaru, Breakdown of broken-symmetry approach to exchange interaction, *J. Chem. Phys.*, 2025, **162**, 164701.
33 E. Ruiz, J. Cano, S. Alvarez and P. Alemany, Broken symmetry approach to calculation of exchange coupling constants for homobinuclear and heterobinuclear transition metal complexes, *J. Comput. Chem.*, 1999, **20**, 1391–1400.
34 G. Singh, S. Gamboa, M. Orio, D. A. Pantazis and M. Roemelt, Magnetic exchange coupling in Cu dimers studied with modern multireference methods and broken-symmetry coupled cluster theory, *Theor. Chem. Acc.*, 2021, **140**, 139.
35 T. Nakamura, T. Kanetomo and T. Ishida, Strong Antiferromagnetic Interaction in a Gadolinium(III) Complex with Methoxy-TEMPO Radical: A Relation between the Coupling and the Gd–O–N Angle, *Inorg. Chem.*, 2021, **60**, 535–539.
36 T. Gupta, T. Rajeshkumar and G. Rajaraman, Magnetic exchange in {Gd^{III}–radical} complexes: method assessment, mechanism of coupling and magneto-structural correlations, *Phys. Chem. Chem. Phys.*, 2014, **16**, 14568–14577.
37 L. E. Roy and T. Hughbanks, Magnetic Coupling in Dinuclear Gd Complexes, *J. Am. Chem. Soc.*, 2006, **128**, 568–575.
38 J. Corredoira-Vázquez, C. González-Barreira, M. Fondo, A. M. García-Deibe, J. Sanmartín-Matalobos, S. Gómez-Coca, E. Ruiz and E. Colacio, Dinuclear Fluoride Single-Bridged Lanthanoid Complexes as Molecule Magnets: Unprecedented Coupling Constant in a Fluoride-Bridged Gadolinium Compound, *Inorg. Chem.*, 2022, **61**, 9946–9959.
39 G. Brunet, F. Habib, I. Korobkov and M. Murugesu, Slow Magnetic Relaxation Observed in Dysprosium Compounds Containing Unsupported Near-Linear Hydroxo- and Fluoro-Bridges, *Inorg. Chem.*, 2015, **54**, 6195–6202.
40 Z. Xie, K. Chui, Q. Yang, T. C. W. Mak and J. Sun, Synthesis, Molecular Structure, and Reactivity of Organolanthanide Fluoride Complexes, $[\{(Me_3Si)_2C_5H_3\}_2Ln(\mu\text{-}F)]_2$ (Ln = La, Nd, Sm, Gd) and $[(C_5H_5)_2Ln(\mu\text{-}F)(THF)]_2$ (Ln = Y, Yb), *Organometallics*, 1998, **17**, 3937–3944.
41 Y. Huo, Y.-C. Chen, S.-G. Wu, J.-L. Liu, J.-H. Jia, W.-B. Chen, B.-L. Wang, Y.-Q. Zhang and M.-L. Tong, Effect of Bridging Ligands on Magnetic Behavior in Dinuclear Dysprosium Cores Supported by Polyoxometalates, *Inorg. Chem.*, 2019, **58**, 1301–1308.
42 W. J. Evans, D. G. Giarikos, M. A. Johnston, M. A. Greci and J. W. Ziller, Reactivity of the europium hexafluoroacetylacetonate (hfac) complex, Eu(hfac)3(diglyme), and related analogs with potassium: formation of the fluoride hfac ''ate'' complexes, [LnF(hfac)3K(diglyme)]2, *J. Chem. Soc., Dalton Trans.*, 2002, 520–526.
43 Y.-B. Lu, J.-W. Wu, S.-D. Zhu, S.-Q. Wang, S.-Y. Zhang, C.-M. Liu, R. Li, J. Li, J.-H. Ai and Y.-R. Xie, 3-Pyridylacetic-Based Lanthanide Complexes Exhibiting Magnetic Entropy Changes, Single-Molecule Magnet, and Fluorescence, *ACS Omega*, 2022, **7**, 2604–2612.
44 A. Rasamsetty, S. Mehta, K. U. Ansari, P. Kumar, A. Mondal and M. Shanmugam, Six-coordinated dinuclear lanthanide(III) amide complexes: investigation of magnetization relaxation dynamics and their electronic structures, *Dalton Trans.*, 2022, **51**, 63–68.
45 T. Han, Y.-S. Ding, Z.-H. Li, K.-X. Yu, Y.-Q. Zhai, N. F. Chilton and Y.-Z. Zheng, A dichlorido-bridged dinuclear Dy(III) single-molecule magnet with an effective energy barrier larger than 600 K, *Chem. Commun.*, 2019, **55**, 7930–7933.
46 L. Dong, Y.-B. Lu, S.-D. Zhu, J.-W. Wu, X.-T. Zhang, Y. Liao, C.-M. Liu, S.-J. Liu, Y.-R. Xie and S.-Y. Zhang, A new family of dinuclear lanthanide complexes exhibiting luminescence, magnetic entropy changes and single molecule magnet behaviors, *CrystEngComm*, 2021, **23**, 645–652.
47 D. Lüert, A.-K. Kreyenschmidt, C. M. Legendre, R. Herbst-Irmer and D. Stalke, A Sodium Sodate as Precursor for Lanthanide Bis(4-*R*-benzoxazol-2-yl)methanide Single-Molecule Magnets, *Inorg. Chem.*, 2022, **61**, 5234–5244.
48 W. Lamberts, H. Lueken and U. Elsenhans, Structural chemistry of lanthanidedicyclopentadienidehalides. Part 1. Two modifications of gadoliniumdicyclopentadienidebromide, $[Gd(C_5H5)_2Br]_2$ and $1\infty[Gd(C_5H_5)_2Br]$, *Inorg. Chim. Acta*, 1986, **121**, 81–87.
49 M. Li, H. Wu, Z. Xia, V. Montigaud, O. Cador, B. Le Guennic, H. Ke, W. Wang, G. Xie and S. Chen, Bromine-bridged Dy2 single-molecule magnet: magnetic anisotropy driven by cis/trans stereoisomers, *Chem. Commun.*, 2019, **55**, 14661–14664.
50 C. A. Gould, K. R. McClain, D. Reta, J. G. C. Kragskow, D. A. Marchiori, E. Lachman, E.-S. Choi, J. G. Analytis, R. D. Britt, N. F. Chilton, B. G. Harvey and J. R. Long, Ultrahard magnetism from mixed-valence dilanthanide complexes with metal-metal bonding, *Science*, 2022, **375**, 198–202.
51 J. Locher, S. J. Gross, C. Zacharias, S. Dechert, S. Demeshko and L. Vondung, Lanthanum and gadolinium complexes with neutral tertiary phosphine ligands: synthesis, structures, magnetism and bonding, *Dalton Trans.*, 2026, DOI: 10.1039.D6DT01324D.
52 J. Jung, F. Benner, R. Herbst-Irmer, S. Demir and D. Stalke, Slow Magnetic Relaxation in Mono- and Bimetallic Lanthanide Tetraimido-Sulfate $S(NtBu)_4^{2-}$ Complexes, *Chem. – Eur. J.*, 2021, **27**, 12310–12319.
53 K. S. Pedersen, G. Lorusso, J. J. Morales, T. Weyhermüller, S. Piligkos, S. K. Singh, D. Larsen, M. Schau-Magnussen, G. Rajaraman, M. Evangelisti and J. Bendix, Fluoride-Bridged $\{Gd^{III}{}_3M^{III}{}_2\}$ (M = Cr, Fe, Ga) Molecular Magnetic Refrigerants, *Angew. Chem., Int. Ed.*, 2014, **53**, 2394–2397.
54 G. B. Deacon, D. J. Evans, P. C. Junk, E. Lork, R. Mews and B. Žemva, Stabilising small clusters: synthesis and

characterisation of thermolabile $[Gd_4F_7(15\text{-crown-}5)_4][AsF_6]_5 \cdot 6SO_2$, *Dalton Trans.*, 2005, 2237.
55 D. A. Buschmann, H. M. Dietrich, J. Durrant, C. Maichle-Mössmer, J. Tang, R. A. Layfield and R. Anwander, Multimetallic Half-Sandwich Complexes of the Rare-Earth Metals, *Inorg. Chem.*, 2025, **64**, 2795–2808.
56 R. J. M. Konings and A. Kovács, in *Handbook on the Physics and Chemistry of Rare Earths*, Elsevier, 2003, vol. 33, pp. 147–247.
57 A. Kovács, Theoretical study of rare earth trihalide dimers Ln_2X_6 (Ln = La, Dy; X = F, Cl, Br, I), *Chem. Phys. Lett.*, 2000, **319**, 238–246.
58 A. Kovács, Selected structural highlights of f-element compounds, *Struct. Chem.*, 2025, **36**, 1557–1575.
59 S. G. Balasubramani, G. P. Chen, S. Coriani, M. Diedenhofen, M. S. Frank, Y. J. Franzke, F. Furche, R. Grotjahn, M. E. Harding, C. Hättig, A. Hellweg, B. Helmich-Paris, C. Holzer, U. Huniar, M. Kaupp, A. Marefat Khah, S. Karbalaei Khani, T. Müller, F. Mack, B. D. Nguyen, S. M. Parker, E. Perlt, D. Rappoport, K. Reiter, S. Roy, M. Rückert, G. Schmitz, M. Sierka, E. Tapavicza, D. P. Tew, C. van Wüllen, V. K. Voora, F. Weigend, A. Wodynski and J. M. Yu, TURBOMOLE: Modular program suite for ab initio quantum-chemical and condensed-matter simulations, *J. Chem. Phys.*, 2020, **152**, 184107.
60 D. Peng, N. Middendorf, F. Weigend and M. Reiher, An efficient implementation of two-component relativistic exact-decoupling methods for large molecules, *J. Chem. Phys.*, 2013, **138**, 184105.
61 P. Pollak and F. Weigend, Segmented Contracted Error-Consistent Basis Sets of Double- and Triple-ζ Valence Quality for One- and Two-Component Relativistic All-Electron Calculations, *J. Chem. Theory Comput.*, 2017, **13**, 3696–3705.
62 A. D. Becke, A new mixing of Hartree–Fock and local density-functional theories, *J. Chem. Phys.*, 1993, **98**, 1372–1377.
63 K. Eichkorn, O. Treutler, H. Öhm, M. Häser and R. Ahlrichs, Auxiliary basis sets to approximate Coulomb potentials, *Chem. Phys. Lett.*, 1995, **240**, 283–290.
64 C. Adamo and V. Barone, Toward reliable density functional methods without adjustable parameters: The PBE0 model, *J. Chem. Phys.*, 1999, **110**, 6158–6170.
65 T. Yanai, D. P. Tew and N. C. Handy, A new hybrid exchange–correlation functional using the Coulomb-attenuating method (CAM-B3LYP), *Chem. Phys. Lett.*, 2004, **393**, 51–57.
66 J.-D. Chai and M. Head-Gordon, Systematic optimization of long-range corrected hybrid density functionals, *J. Chem. Phys.*, 2008, **128**, 084106.
67 M. Cranmer, Interpretable Machine Learning for Science with PySR and SymbolicRegression.jl, *arXiv*, 2023, preprint, arXiv:2305.01582, DOI: 10.48550/arXiv.2305.01582.
68 J. O. Spiegel and J. D. Durrant, AutoGrow4: an open-source genetic algorithm for de novo drug design and lead optimization, *J. Cheminform.*, 2020, **12**, 25.
69 M. Sierka, J. Döbler, J. Sauer, G. Santambrogio, M. Brümmer, L. Wöste, E. Janssens, G. Meijer and K. R. Asmis, Unexpected Structures of Aluminum Oxide Clusters in the Gas Phase, *Angew. Chem., Int. Ed.*, 2007, **46**, 3372–3375.
70 The pandas development team, 2025.
71 C. Au and R. Au, The crystal structure of $GdCl_3$, *Acta Crystallogr.*, 1967, **23**, 1112.
72 L. Qin, G.-J. Zhou, Y.-Z. Yu, H. Nojiri, C. Schröder, R. E. P. Winpenny and Y.-Z. Zheng, Topological Self-Assembly of Highly Symmetric Lanthanide Clusters: A Magnetic Study of Exchange-Coupling ''Fingerprints'' in Giant Gadolinium(III) Cages, *J. Am. Chem. Soc.*, 2017, **139**, 16405–16411.
73 K. Fink, C. Wang and V. Staemmler, Ab initio calculations of the magnetic exchange coupling in sulfur-bridged binuclear Ni(II) complexes, *Int. J. Quantum Chem.*, 1997, **65**, 633–641.
74 S. Gamboa-Ramirez, K. Youssef, R. Papadakis, M. Giorgi, S. Bertaina, A. J. Simaan and M. Orio, A Three-Dimensional Structural Model for Predicting Magnetic Exchange and Hydrogen Positions in Bis-μ-Hydroxido Cu(II) Dimers, *Eur. J. Inorg. Chem.*, 2026, e202500589.
75 C. Wang, K. Fink and V. Staemmler, An ab initio study of the geometry dependence of the magnetic exchange coupling in oxo-bridged binuclear chromium(III) complexes, *Chem. Phys.*, 1995, **201**, 87–94.
76 Z. Chen, Z. Xu, L. Zhang, F. Yan and Z. Lin, Magnetic Exchange Interactions in Oxo-Bridged Diiron(III) Systems: Density Functional Calculations Coupling the Broken Symmetry Approach, *J. Phys. Chem. A*, 2001, **105**, 9710–9716.
77 H. Schurkus, D.-T. Chen, H.-P. Cheng, G. Chan and J. Stanton, Theoretical prediction of magnetic exchange coupling constants from broken-symmetry coupled cluster calculations, *J. Chem. Phys.*, 2020, **152**, 234115.
78 P. S. Koroteev, N. N. Efimov, Zh. V. Dobrokhotova, I. G. Fomina, A. B. Ilyukhin, I. L. Eremenko and V. M. Novotortsev, Magnetostructural correlation for the Gd complexes with bridging oxygen, *Russ. Chem. Bull.*, 2013, **62**, 1768–1771.
79 S. Roy, P. Shukla, N. Ahmed, M.-H. Du, I. Tarannum, X.-J. Kong, T. Gupta, S. K. Singh and S. Das, Interplay between anisotropy and magnetic exchange to modulate the magnetic relaxation behaviours of phenoxo bridged Dy2 dimers with axial β-diketonate co-ligands, *Dalton Trans.*, 2022, **51**, 18187–18202.
80 L. H. Ahrens, The use of ionization potentials Part 1. Ionic radii of the elements, *Geochim. Cosmochim. Acta*, 1952, **2**, 155–169.
81 G. T. Nguyen and L. Ungur, in *Computational Modelling of Molecular Nanomagnets*, ed. G. Rajaraman, Springer International Publishing, Cham, 2023, vol. 34, pp. 111–153.
82 O. Kahn, *Molecular magnetism*, VCH, Weinheim New York Cambridge, 1993.
83 A. E. Reed, R. B. Weinstock and F. Weinhold, Natural population analysis, *J. Chem. Phys.*, 1985, **83**, 735–746.
84 T. Rajeshkumar, R. Jose, P. R. Remya and G. Rajaraman, Theoretical Studies on Trinuclear $\{Mn^{III}_2Gd^{III}\}$ and Tetranuclear $\{Mn^{III}_2Gd^{III}_2\}$ Clusters: Magnetic Exchange, Mechanism of

 This journal is © the Owner Societies 2026

Magnetic Coupling, Magnetocaloric Effect, and Magneto–Structural Correlations, *Inorg. Chem.*, 2019, **58**, 11927–11940.
85 S. K. Singh and G. Rajaraman, Decisive interactions that determine ferro/antiferromagnetic coupling in {3d–4f} pairs: a case study on dinuclear {V(IV)–Gd(III)} complexes, *Dalton Trans.*, 2013, **42**, 3623.
86 O. F. Fellner, K. Kotrle, E. Čižmár, J. Brázdová, P. Štarha, J. Moncoľ, R. Herchel and I. Nemec, Influence of Carboxylate Ligand Variation on Structure, Magnetic Exchange, and Magnetocaloric Performance in Hexanuclear Gd(III) Complexes, *Chem. – Eur. J.*, 2026, **32**, e03579.